

PAPER • OPEN ACCESS

Multiple metamagnetism, extreme magnetoresistance and nontrivial topological electronic structures in the magnetic semimetal candidate holmium monobismuthide

To cite this article: Z M Wu *et al* 2019 *New J. Phys.* **21** 093063

View the [article online](#) for updates and enhancements.

You may also like

- [Ferromagnetic and Superparamagnetic Contributions in the Magnetoresistance of Electrodeposited Co-Cu/Cu Multilayers](#)
Qun-Xian Liu, László Péter, József Pádár et al.
- [Satellite-based links for quantum key distribution: beam effects and weather dependence](#)
Carlo Liorni, Hermann Kampermann and Dagmar Bruß
- [Engineering effective Hamiltonians](#)
Holger Haas, Daniel Puzzuoli, Feihao Zhang et al.



PAPER

Multiple metamagnetism, extreme magnetoresistance and nontrivial topological electronic structures in the magnetic semimetal candidate holmium monobismuthide

OPEN ACCESS

RECEIVED
19 May 2019REVISED
21 August 2019ACCEPTED FOR PUBLICATION
12 September 2019PUBLISHED
30 September 2019

Original content from this work may be used under the terms of the [Creative Commons Attribution 3.0 licence](#).

Any further distribution of this work must maintain attribution to the author(s) and the title of the work, journal citation and DOI.

Z M Wu^{1,5}, Y R Ruan^{2,3,5}, F Tang^{1,4}, L Zhang¹ , Y Fang^{1,6} , J-M Zhang^{2,3,6} , Z D Han¹, R J Tang⁴ , B Qian^{1,6} and X F Jiang¹

¹ Jiangsu Laboratory of Advanced Functional Materials, Department of Physics, Changshu Institute of Technology, Changshu 215500, People's Republic of China

² Fujian Provincial Key Laboratory of Quantum Manipulation and New Energy Materials, College of Physics and Energy, Fujian Normal University, Fuzhou 350117, People's Republic of China

³ Fujian Provincial Collaborative Innovation Center for Optoelectronic Semiconductors and Efficient Devices, Xiamen 361005, People's Republic of China

⁴ Jiangsu Key Laboratory of Thin Films, School of Physical Science and Technology, Soochow University, Suzhou 215006, People's Republic of China

⁵ ZMW and YRR contributed equally to this work.

⁶ Authors to whom any correspondence should be addressed.

E-mail: fangyong@cslg.edu.cn, jmzhang@fjnu.edu.cn and njqb@cslg.edu.cn

Keywords: magnetism, magnetoresistance, semimetal, first-principle calculation

Supplementary material for this article is available [online](#)

Abstract

Inconceivably large changes (up to 10⁶%) of the resistivity induced by external magnetic field—a phenomenon known as the extreme magnetoresistance effect has been reported in a great number of exotic semimetals. The very recent and exciting discoveries mainly pay attention to the compounds without magnetic ground states, which appears to limit the potential growth of semimetal family. For fundamental scientific interests, introduction of spin degree of freedom would provide an almost ideal platform for investigating the correlation effect between magnetism, crystallographic structure and electric resistivity in materials. Here, we report the experimental observation of metamagnetic behaviors and transport properties of HoBi single crystals. Being a magnetic member of the rare earth mononictide family, the magnetoresistance of HoBi is significantly modulated by the magnetic orders at low temperature, which shows a nonmonotonic increment across the successive magnetic phases and reaches 10⁴% (9 T and 2 K) in the ferromagnetic state. Kohler's rule predicts that more than one type of carriers dominates the transport properties. Well fitted magnetoresistance and Hall resistivity curves by the semiclassical two-band model suggest that the densities of electron and hole carriers are nearly compensated and the carrier mobilities in this compound are ultrahigh. Besides, the inverted band structures and nonzero Z_2 topological invariant indicate that possible nontrivial electronic states could generate in the ferromagnetic phase of HoBi. Combining the experimental and theoretical results, it is found that the cooperative action of carrier compensation effect and ultrahigh mobility might contribute to the extreme magnetoresistance observed in the titled compound. These findings suggest a paradigm for obtaining the extreme magnetoresistance in magnetic compounds and are relevant to understand the rare-earth-based correlated topological materials.

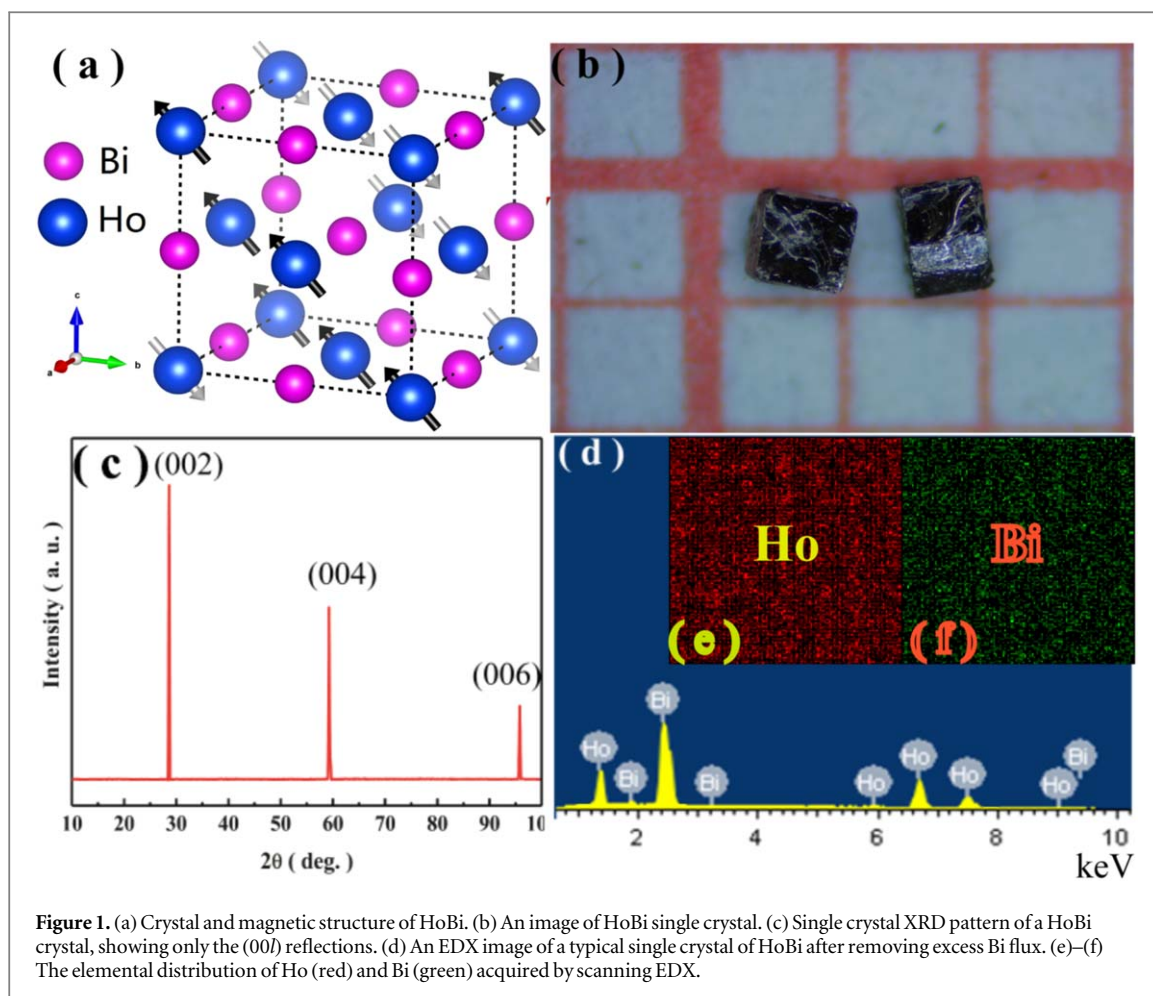
1. Introduction

Magnetoresistance (MR), which means that the resistance of materials can be tuned by external magnetic field, brings revolution to modern industry through its device applications, such as magnetic sensors, hard drives and so on [1]. Besides the anisotropic magnetoresistance, giant magnetoresistance, colossal magnetoresistance and

tunnel magnetoresistance [2–5], extremely large magnetoresistance have attracted increasing interest [6, 7], since it not only offer the potential to design new devices, but also pose challenges to understand the fundamental phenomena in nature. The extreme magnetoresistance has been widely reported in the classic elemental semimetal Bi, topological semimetals WTe_2 , Cd_3As_2 , TaPn (Pn = As, Sb) family, pyrite-type $PtBi_2$, $RPtBi$ ($R = Nd, Gd$), RPn ($R = \text{rare earth; Pn} = Sb, Bi$) and so on [8–30]. Ever since the unprecedentedly large magnetoresistance is revealed in LaSb, the research enthusiasm on rare earth monopnictides RPn ($R = \text{rare earth, Pn} = Sb, Bi$) is inspired [16–30]. The family has been widely studied in the 1980–90s for its heavy-fermion nature [31]. Intriguingly, the recent calculations predict that LaPn (Pn = N, P, As, Sb, and Bi) could be a topological prototype material with band inversion at X point of the bulk *fcc* Brillouin zone [32]. Afterwards, further investigation on this family has been systematically performed [17–30]. It is found that some members of this family have topologically nontrivial band structures. The angle-resolved photoelectron spectroscopy (ARPES) and first-principle calculations provide clear evidence of topologically nontrivial surface states for LaBi [33]. The nontrivial Z_2 invariant obtained in YBi also suggests that it is a potential topological semimetal candidate [28]. A noticeable fact is that most of the topological semimetals are found to be nonmagnetic [34]. Actually, materials with spin degree of freedom are involved in the initial proposals of topological semimetals, where the spin degeneracy of bands can be lifted by breaking the time-reversal symmetry [35]. For absence of high-quality samples, it is hard to observe the topological states in magnetic semimetals [26]. Thanks to the advances in crystal growth techniques, the rare earth monopnictides with partially filled *f* shells provide possibilities to study the exotic properties. For example, chiral-anomaly-related negative magnetoresistance observed in NdSb indicates that this antiferromagnetic compound is a Dirac semimetal [26]. Nontrivial Berry phase obtained in the ferromagnetic state of HoSb indirectly reveals its topological nature as well [36]. Bulk-sensitive soft x-ray ARPES confirms that CeBi is topologically nontrivial by observation of its band inversion [37]. Besides, ferromagnetic GdSb is speculated to be a Weyl semimetal candidate, which still needs further experimental confirmation [38]. It should be noted that the rare earth ions with partially filled *f* shells possess not only magnetic orders, but also strong electronic correlations. Especially, as a result of the electronic correlation, various exotic physical properties could be expected in the rare-earth-based semimetals. Take $RPtBi$ ($R = Nd, Gd$) as an example, due to the large exchange field arising from *4f* electrons of *R* ion and the Zeeman splitting in the presence of magnetic field, the bands split and form Weyl points near the Fermi level, which induces negative magnetoresistance, huge anomalous Hall conductivity and planar Hall effect [13–15]. As this scenario shows, strong electronic correlations open the possibility of discovering completely new states of matter with unprecedented functionality, which could also be expected in the magnetic rare earth monopnictides.

HoBi, which adopts the rocksalt-type structure at room temperature (figure 1(a)), namely cubic symmetry with space group $Fm\bar{3}m$ [39], is another representative of the rare earth monopnictide family. The trivalent Ho, which is generally described as a non-Kramers ion with total spin moment $S = 2$ and orbital moment $L = 6$, has relatively dominant orbital contribution, resulting in strongly anisotropic magnetism in the titled compound [39]. Earlier neutron diffraction experiments showed that HoBi underwent a first order transition to *fcc*-type antiferromagnetism at low temperature [40]. Magnetic measurement performed by Hulliger *et al* found that this compound experienced several magnetic states associated with significant hysteresis in most transitions [39]. While, Fente *et al* reported that no hysteresis emerged during the evolution of magnetization as a function of field [40]. Beyond that complicated magnetic orders, recent studies have also drawn attention to the magnetotransport of HoBi [29]. Neutron diffraction reveals that the $(1/6, 1/6, 1/6)$ ordered state could significantly affect the resistivity along $[110]$ direction in the intermediate fields and the $(0, 0, 0)$ polarized state drives the occurrence of extreme magnetoresistance [29]. As reported, the magnetic phase diagram in the $[001]$ direction is more complicated comparing to that along the $[110]$ direction, indicating that different transport properties can be expected in the former magnetic states.

Here, we aim to reevaluate the magnetic transitions, and uncover the origin of extremely large magnetoresistance in HoBi single crystal. As expected, anisotropic magnetism and multiple metamagnetic transitions with significant hysteresis are identified in this compound. After all the phase transitions evolve completely, the ferromagnetic states form, where the extreme change of resistivity with an order of $10^4\%$ is obtained. The magnetoresistance curves can be nicely fitted by the semiclassical two-band model, indicating that the electron and hole carriers in HoBi are nearly compensated. First-principle calculations confirm that this compound is indeed a semimetal and several electron pockets and hole pockets coexist. Furthermore, the nontrivial electronic structure of HoBi is also evaluated, which hosts inverted band structure and nonzero topological invariant. Electron–hole compensation effect along with ultrahigh carrier mobility, could contribute to the extreme magnetoresistance in HoBi.



2. Experimental

2.1. Sample growth and chemical characterization

Single crystals of HoBi were grown from the Bi flux method. Highly purified crude materials of Ho and Bi with a molar ratio of 1:19 were put into a tantalum crucible and then sealed in an evacuated quartz tube. All the operation was conducted in an argon-filled glove box, where the oxygen and humidity content were less than 0.1 ppm. The quartz tube was heated to 1273 K, held for 24 h, and followed by slow cooling to 773 K at a rate of 0.5 K h^{-1} in furnace. At this temperature, the excess Bi flux was removed by centrifugation. Then, shiny and cubic single crystals (figure 1(b)) were obtained. To determine the crystal structure and phase purity, x-ray diffraction (XRD) with Cu *K* α radiation was performed with 2θ ranging from 10° to 100° at room temperature. Chemical stoichiometry of the polished crystals was characterized by a Zeiss Sigma field emission scanning electronic microscopy equipped with an Oxford INCA energy-dispersive x-ray spectrometer (EDX).

2.2. Magnetization and transport measurements

The temperature- and field-dependent magnetization measurements were carried out using the VSM module of a physical property measurement system (PPMS-VSM, Quantum Design), where the temperature and magnetic field vary from 2 to 300 K and from 0 to 9 T, respectively. The electric resistivity and Hall effect measurements were performed in a temperature ranging from 2 to 300 K and in an applied magnetic field up to 9 T on a Quantum Design PPMS platform. For all the electric measurement, standard four-probe method was used.

2.3. Band structure and fermi surface calculations

Band structure and Fermi surface of HoBi were built by first-principles calculations implemented in the Vienna *ab initio* simulation package code, where the projected augmented wave method and Perdew–Burke–Ernzerhof (PBE) type exchange–correlation interactions were employed [41, 42]. The plan-wave cutoff energy of 600 eV and a $30 \times 30 \times 30$ Gamma-centered *K*-mesh were adopted in the electronic structure calculation. Spin–orbit coupling and on-site Hubbard *U* for the correlated 4*f*-electrons were included in all calculations with $U = 7 \text{ eV}$, $J = 0.6 \text{ eV}$. The lattice constants $a = b = c$ of HoBi were taken as 6.223 Å. The optimization procedure was

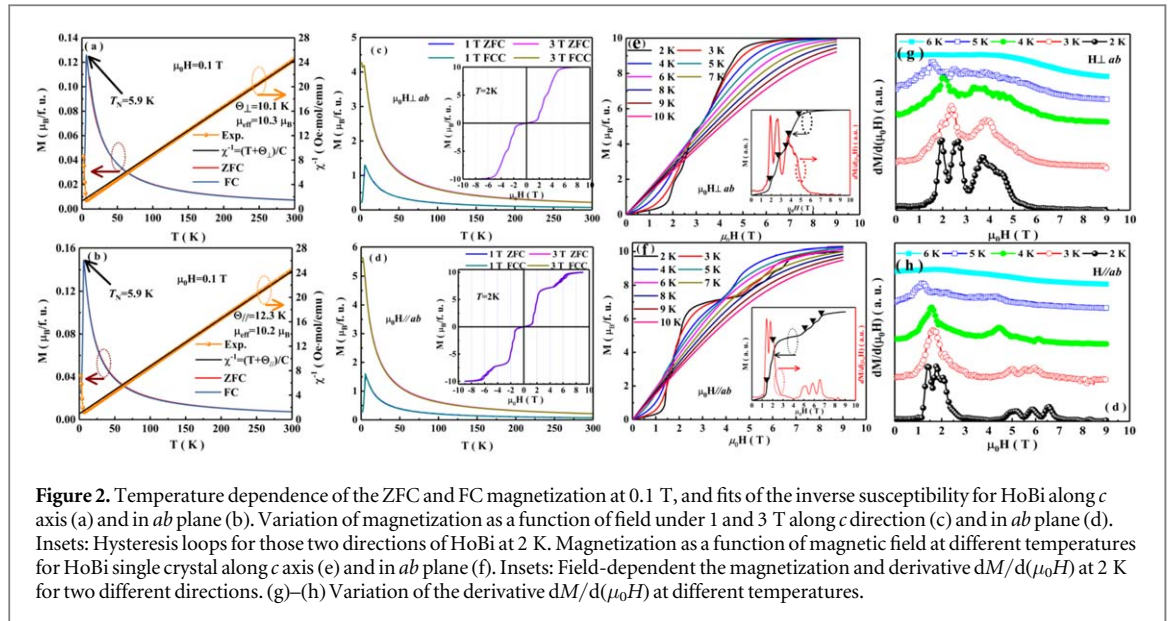


Figure 2. Temperature dependence of the ZFC and FC magnetization at 0.1 T, and fits of the inverse susceptibility for HoBi along *c* axis (a) and in *ab* plane (b). Variation of magnetization as a function of field under 1 and 3 T along *c* direction (c) and in *ab* plane (d). Insets: Hysteresis loops for those two directions of HoBi at 2 K. Magnetization as a function of magnetic field at different temperatures for HoBi single crystal along *c* axis (e) and in *ab* plane (f). Insets: Field-dependent magnetization and derivative $dM/d(\mu_0H)$ at 2 K for two different directions. (g)–(h) Variation of the derivative $dM/d(\mu_0H)$ at different temperatures.

truncated until the residual forces for each relaxed atoms were less than $0.02 \text{ eV } \text{\AA}^{-1}$. Considering that the band gap determined by the generalized gradient approximations (GGA) was possibly overestimated, a hybrid functional approximation for the exchange–correlation with Heyd–Scuseria–Ernzerhof (HSE06) was supplemented to further examine the relativistic effect on band structure [43].

3. Results and discussion

3.1. Structural and elementary composition analysis

Figure 1(c) shows the XRD pattern for HoBi single crystal along the (001) plane. Sharp peaks (00*h*) in the diffraction spectrum indicate high crystalline nature of the grown crystals. The composition of well-polished single crystal is determined by EDX spectroscopy, which is carried out at different positions on the crystal surfaces with an instrument error of 1%–2%. Typical results plotted in figure 1(d) confirm almost the perfect stoichiometry (Ho:Bi = 49.8:50.2), and no evidence of Bi thin film or nanocluster in the as-grown crystals. As shown in figures 1(e) and (f), Ho and Bi are uniformly distributed across the crystal surface, suggesting an absence of any observable impurity as well.

3.2. Measurement of magnetic property

The thermomagnetic curves of HoBi single crystal in zero-field-cooled (ZFC) and field-cooled (FC) modes are measured under an external field of 0.1 T perpendicular (figure 2(a)) and parallel (figure 2(b)) to *ab* plane. As shown in figure 2(a), the magnetization along *c*-axis shows an antiferromagnetic transition at 5.9 K (Néel temperature T_N), which is consistent with the previous works [40, 41]. The ZFC and FC magnetization curves almost superimpose in the whole measured temperature range (2–300 K), indicating the formation of long-range antiferromagnetic orders below Néel temperature. On the other hand, when the magnetic field is applied in *ab* plane, an analogous antiferromagnetic transition is observed at 5.9 K, as displayed in figure 2(b), matching exactly with the Néel temperature as well. The out- and in-plane thermomagnetic curves suggest that antiferromagnetic configurations generate at low temperature, which coincides with the spin structure in figure 1(a). Since the magnetic moments of HoBi mainly originate from Ho ions, as shown in the insets of figures 2(a) and (b), the effective magnetic moments μ_{eff} are estimated to be $10.3 \mu_B$ and $10.2 \mu_B$ by fitting the linear part of inverse magnetic susceptibility $1/\chi(T)$ between 100 and 300 K to Curie–Weiss law $\chi(T) = M/H = C/(T + \Theta)$ with $C = N_A \mu_{\text{eff}}^2 / 3k_B$ (Here, k_B , Θ , C , and μ_B are the Boltzmann constant, Curie–Weiss temperature, Curie constants and Bohr magneton respectively) [44]. Thereby, the Weiss temperatures are calculated to be $\Theta_{\perp} = 10.1 \text{ K}$ and $\Theta_{\parallel} = 12.3 \text{ K}$. The difference in two susceptibilities indicates the remarkable magnetic anisotropy in HoBi, which is confirmed by the magnetic hysteresis loops shown below as well. Figures 2(c) and (d) show the ZFC and FC magnetization as a function of temperature under 1 and 3 T. It is clear that, other than the obviously enhanced magnetization, the antiferromagnetic orders remain persistent at 1 T, exhibiting a transition from paramagnetism to antiferromagnetism at low temperature. When a higher field (3 T) is applied, slightly different magnetization responses to the applied magnetic field can be observed in the two directions. As plotted in figure 2(d), the antiferromagnetic order is suppressed and a remarkable phase

transition from paramagnetic to ferromagnetic-like state takes shape. In figure 2(c), the ferromagnetic-like phase has not completely formed, and a cusp, which is a generic feature of antiferromagnetic transition, still exists around the magnetic transition temperature. The insets of figures 2(c) and (d) illustrate the magnetic hysteresis loops of HoBi at 2 K. As shown, obvious metamagnetic behaviors are observed, where the onset fields for those transitions in the two directions are disparate. Furthermore, a significant hysteresis, which doesn't develop in the inset of figure 2(c), is evidenced in the inset of figure 2(d), showing an anisotropic behavior of magnetization. It is noticed that the magnetization of HoBi is saturated above 5 and 7 T, i.e. $\mu_{\text{sat}} = 9.9 \mu_{\text{B}}$ and $10.1 \mu_{\text{B}}$ for the applied field along c axis and in ab plane, which significantly accord with the isolated Hund's rule ground state of Ho^{3+} ion ($10 \mu_{\text{B}}$) [40, 41]. As is reported, $R\text{Pn}$ ($R = \text{Ce, Dy, Ho; Pn}=\text{Sb, Bi}$) shows metamagnetic transitions with diverse behaviors below the antiferromagnetic temperature [24, 36, 40, 45]. For instance, DySb shows a plateau at one half of the saturated moment in an intermediate phase between 2.5 and 4.2 T, which is ascribed to the competition between Zeeman effect and magnetocrystalline anisotropy [24]. More narrowly, DySb is a type-II antiferromagnet and its ground state can be driven into ferromagnetic state via a HoP-type intermediate phase, where the moment in one of each two nearest ferromagnetic plane are rotated 90° and the measured magnetization is one half of the saturated values, by applying a magnetic field along the easy axis direction [24]. Analogous metamagnetic transitions are observed in HoSb, in which the MnO-type antiferromagnetic ground state also goes through a HoP-type spin structure to a ferromagnetic spin structure with the increasing magnetic field [36]. Relatively speaking, the metamagnetic transition of HoBi shown in the inset of figures 2(c) and (d) are more complicated, indicating that richer magnetic phase diagram could be expected.

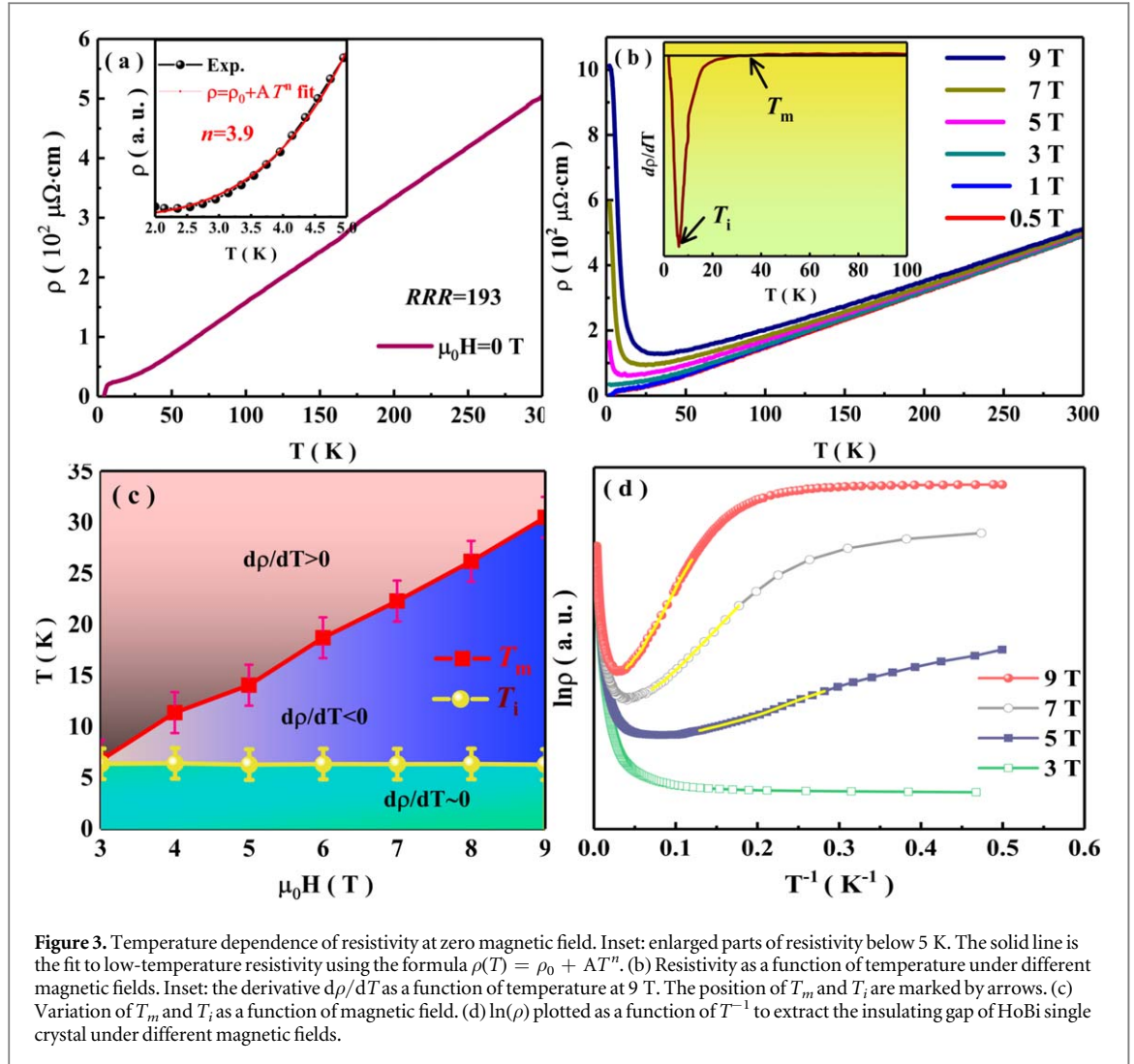
To study the metamagnetic properties of HoBi in detail, the magnetization as a function of magnetic field along different directions are plotted in figures 2(e) and (f). Clearly, the anisotropy of HoBi is reinforced again, where the isothermal magnetization curves show different shapes and critical fields for those magnetic transitions. As shown, several field-induced magnetically ordered phases can be readily observed at low temperature. Actually, to precisely determine the magnetic transitions, neutron diffraction on this compound is necessary, which is unavailable to us at the moment. Here, the critical fields for metamagnetic transitions in HoBi are roughly determined from the peaks in derivative $dM/d(\mu_0H)$. There are approximately five maximums at low temperature [40]. For clarity, the insets of figures 2(e) and (f) plot the field dependence of magnetization and $dM/d(\mu_0H)$ at 2 K. The magnetization jumps rapidly at 1.9, 2.5, 3.7, 4.2, and 4.8 T in the inset of figure 2(e), indicating that the metamagnetic transition is completed under the field less than 5.0 T along c axis. In the inset of figure 2(f), the complicated magnetic transitions at 2 K are mainly distributed in two field regions with a broad valley from 2.5 to 4.6 T in $dM/d(\mu_0H)$ curve. Intriguingly, the applied field can not terminate the metamagnetic transition until 6.5 T, which is slightly larger than that along c axis, reconfirming the remarkable magnetic anisotropy. Figures 2(g) and (h) show the field-dependent derivative $dM/d(\mu_0H)$ at various selected temperatures with the field perpendicular and parallel to ab plane. It can be observed that multiple metamagnetic transitions are induced at low temperature. With the gradual increment of temperature, the metamagnetic behaviors become more and more inconspicuous, and disappear above 6 K.

3.3. Characterization of the magnetoresistance performance

Figure 3(a) shows the variation of zero-field resistivity with temperature for HoBi from 2 to 300 K. As plotted, the resistivity is metallic in nature and decreases monotonically to 2 K, where the resistivity ρ_0 becomes as small as $2.6 \mu\Omega \text{ cm}$, resulting in a large residual resistivity ratio $RRR = \rho(300 \text{ K})/\rho(2 \text{ K}) \sim 193$. In the inset of figure 3(a), the low-temperature resistivity obeys a power-law behavior, $\rho(T) = \rho_0 + AT^n$ with $n=3.9$ similar in numerical value to that of LaSb ($n = 4$), which indicates the interband s - d e - ph scattering, rather than the intraband s - s e - ph scattering should be dominant [6, 27]. The low-temperature resistivity is also fitted by the above-mentioned relation with $n = 3$ (see the supplementary materials is available online at stacks.iop.org/NJP/21/093063/mmedia). It can be easily found that the fitted curve deviates from the measured one.

Figure 3(b) shows the temperature-dependent resistivity of HoBi at different magnetic fields (0.5, 1, 3, 5, 7, and 9 T). As shown, the low-temperature resistivity is slightly enhanced in the applied magnetic fields of 0.5 T and 1 T. When a larger magnetic field (3, 5, 7, and 9 T) is applied, the low-temperature resistivity significantly increases and experiences a metal-insulator-like behavior along with a minimum at T_m , which is a generic feature of semimetals [16, 19]. The inset of figure 3(b) shows the definition of two characteristic temperatures T_m and T_i , where T_m denotes the point of sign change in $d\rho/dT$, and T_i corresponds to the minimum in $d\rho/dT$ [28].

Figure 3(c) exhibits the evolution of T_m and T_i as a function of magnetic field, in which the former one increases with increasing magnetic field and the latter one is almost field-independent, suggesting that the temperature window of insulator-like regime grows with the increment of applied magnetic field and the temperature of resistivity plateau is field-insensitive [46]. Figure 3(d) shows the plot of T^{-1} -dependent $\log(\rho)$, which can be used to estimate the insulating gap E_g in the insulator-like regime by employing the formula $\rho(T) \sim \exp(E_g/k_B T)$ [16].



The derived values of insulating gap increase monotonically with the increasing magnetic field (not shown), from which sharper metal-insulator crossovers can be expected at higher magnetic field.

Figure 4(a) shows the magnetic field dependence of magnetoresistance for HoBi single crystal at various temperatures, where the external field is applied along c axis and the electric current flows in ab plane (the sketch map is plotted in the inset of figure 4(a)). Obviously, the external field can greatly change the resistivity of HoBi. As displayed in figure 4(a), the positive magnetoresistance reaches an approximate value of $3.9 \times 10^4\%$ at 2 K without any sign of saturation under the magnetic field as large as 9 T. Upon slightly increasing the temperature, the magnetoresistance decreases gradually with its order of magnitude unchanging. At higher temperature, especially above the antiferromagnetic phase temperature about 6 K, the magnetoresistance drops drastically, indicating that the ordered spin structure benefits the generation of extreme magnetoresistance. It can be clearly observed that the magnetoresistance at room temperature (figure 4(a)) is only the order of 4%, which suggests that lattice scattering dominates the electron mobility of HoBi in high temperature regime. Usually, the evolution of resistivity with magnetic field in its sister compounds, like LaBi, YBi, and so on, behaves in a quadratic manner [27, 28]. While, a distinct transport scenario emerges in HoBi, where kinks generate in the magnetoresistance curves. To investigate the origin for occurrence of these features in magnetotransport, the field-dependent magnetoresistance and magnetization at 2 K are replotted in figure 4(b). As shown, the magnetoresistance increases gently under low magnetic field and dramatically changes after 4.6 T. Accordingly, after this critical field, all metamagnetic transitions are completed and HoBi enters its ferromagnetic state, which indicates that the kinks may originate from low-field-induced some magnetic transitions. Similar scenarios in the magnetization and magnetoresistance curves of HoSb have been observed during the evolution of magnetic structure from HoP-type orders to ferromagnetic orders [36]. The correlation effect between the magnetic orders and resistivity of HoBi can be easily reflected in the field-dependent derivative $dMR/d(\mu_0H)$. As shown in figure 4(c), the critical fields (H_C) for inflexions in the magnetoresistance curves increase with the increasing temperature, which also suggests that the ordered low-temperature magnetic states benefit the formation of

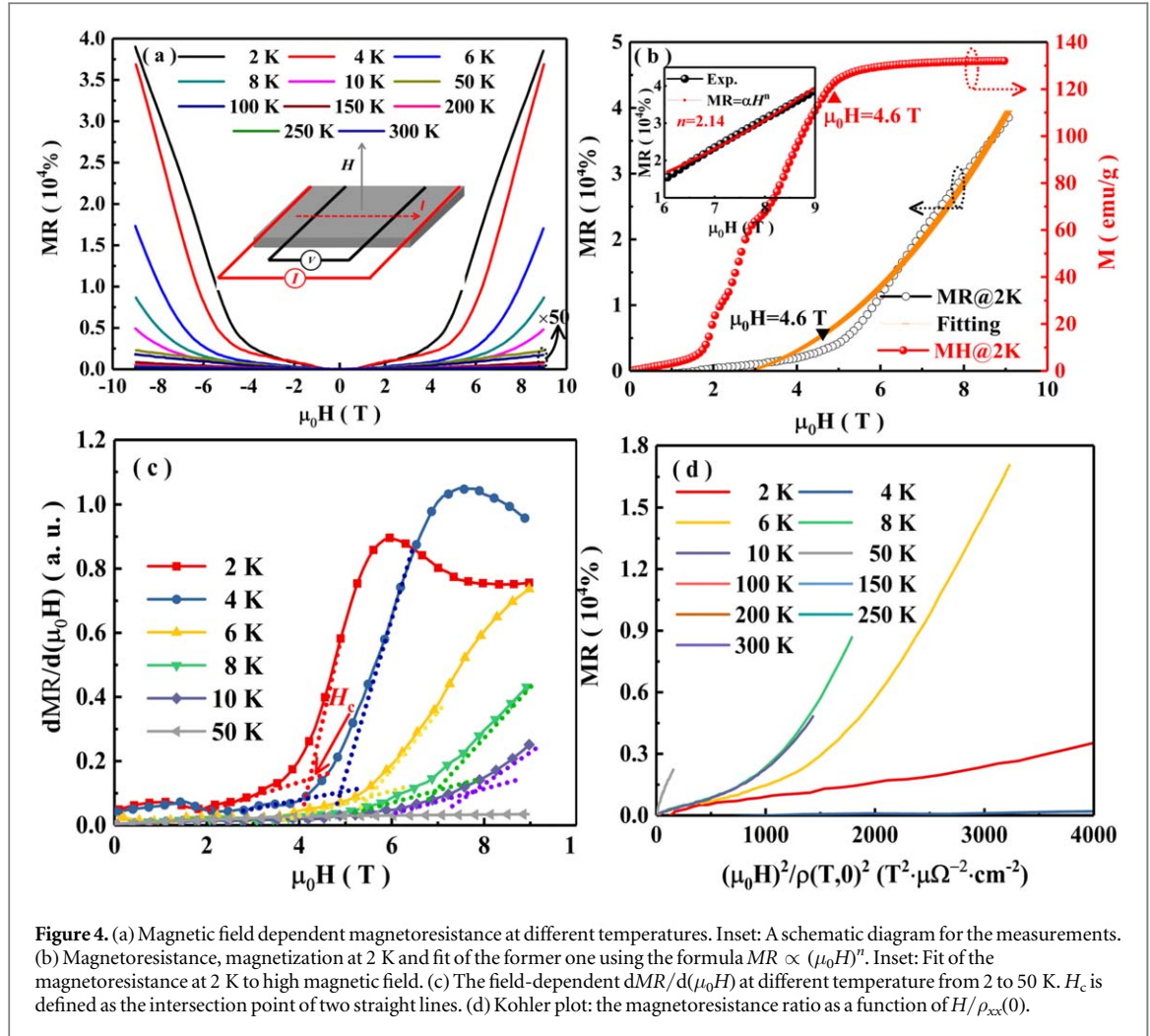


Figure 4. (a) Magnetic field dependent magnetoresistance at different temperatures. Inset: A schematic diagram for the measurements. (b) Magnetoresistance, magnetization at 2 K and fit of the former one using the formula $MR \propto (\mu_0 H)^n$. Inset: Fit of the magnetoresistance at 2 K to high magnetic field. (c) The field-dependent $dMR/d(\mu_0 H)$ at different temperature from 2 to 50 K. H_c is defined as the intersection point of two straight lines. (d) Kohler plot: the magnetoresistance ratio as a function of $H/\rho_{xx}(0)$.

extreme magnetoresistance. Figure 4(d) shows the results of Kohler scaling for magnetoresistance of HoBi. The semiclassical transport theory based on Boltzmann equation predicts that the relative change of resistivity $\Delta\rho/\rho_0$ in a magnetic field is a universal function of H/ρ_0 , $\Delta\rho/\rho_0 = F[H/\rho_0]$, where ρ_0 is the zero-field resistivity at a certain temperature [28]. When there is a single type of charge carrier and relaxation rate τ in the transport process, this rule will be tenable and then all the magnetoresistance isotherms collapse on a single curve. If not, the Kohler's rule will be violated, which has been widely observed in the materials with extreme magnetoresistance, like LaBi, TaPn and TaPn₂ (Pn = As and Sb) [27, 47, 48]. As shown, the magnetoresistance of HoBi obviously deviates from Kohler's rule as well, which may originate from multiband carriers at low temperature, or multiple scattering mechanisms at high temperature. Evidently, as shown in figure 4(b), the field-dependent magnetoresistance at 2 K can be roughly fitted by $MR \propto (\mu_0 H)^n$, where the obtained $n = 2.05$ is closed to 2. Due to the existence of kinks, fitting of the magnetoresistance curve is not perfect. While, as shown in the inset of figure 4(b), the data at high magnetic field can be well fitted, yielding the obtained $n = 2.14$, which is slightly larger than 2 as expected for a perfectly compensated metal. Such deviations have been observed in other materials hosting extreme magnetoresistance as well, like PtSn₄, WTe₂, and some rare earth manopnictides, e.g. LaSb/Bi, NdSb, YSb/Bi, LuSb/Bi [21, 25, 26, 28, 46, 49, 50]. Traditionally, the extremely large magnetoresistance is discussed in the framework of two-band model, which can be expressed as $\rho_{xx} = \frac{(n_e u_e + n_h u_h) + (n_e u_e u_h^2 + n_h u_h u_e^2) B^2}{e[(n_e u_e + n_h u_h)^2 + (u_h - u_e)^2 u_e^2 u_h^2 B^2]}$, where ρ_{xx} is the longitudinal resistivity, e is the electron charge, n is the carrier density, u is the mobility, and the subscripts e and h denote the electron-type and hole-type carriers, respectively [28]. As predicted by this model, the longitudinal resistivity will increase as a function of quadratic in the magnetic field, when the carrier densities of electron and hole are compensated. A slight deviation from the perfect resonant condition can also result in a large quadratic magnetoresistance as long as the applied field is not too strong. In the case of perfect compensation between electrons and holes, another prediction from the formula manifests that the magnetoresistance ratio strongly depends on the average mobility u_{ave} , and can be rewritten as $MR = (u_{ave} B)^2 (u_{ave} = \sqrt{u_e u_h})$ [51]. Based on this formula, the obtained u_{ave} is evaluated to be $2.1 \times 10^4 \text{ cm}^2 \text{ V}^{-1} \text{ s}^{-1}$ at 2 K. Although the average mobility of HoBi stands no superiority with respect to the

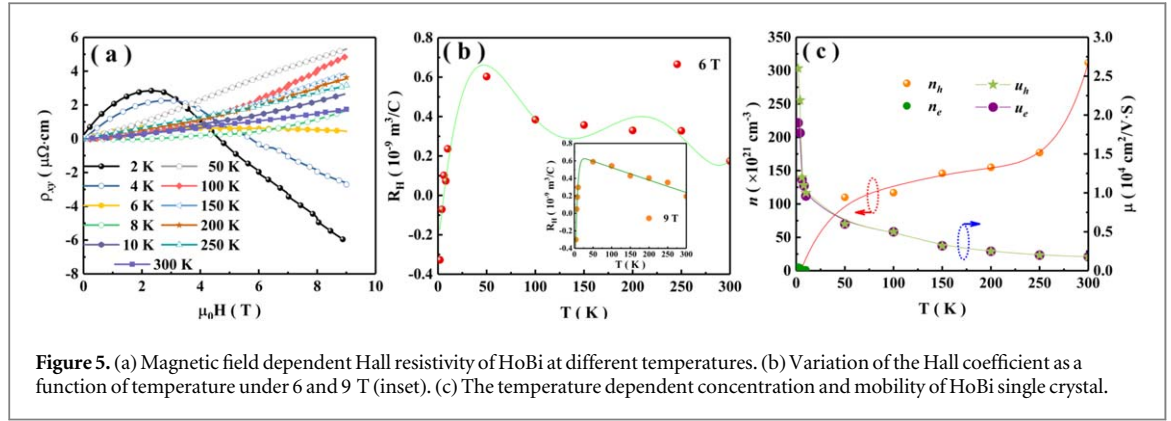


Figure 5. (a) Magnetic field dependent Hall resistivity of HoBi at different temperatures. (b) Variation of the Hall coefficient as a function of temperature under 6 and 9 T (inset). (c) The temperature dependent concentration and mobility of HoBi single crystal.

carrier mobility of topological semimetals like Cd_3As_2 and WTe_2 [52, 53], it is still larger than those of the common magnetic metals, which could contribute to the extreme magnetoresistance of this compound.

3.4. Hall effect measurement

To evaluate the carrier densities and mobilities of HoBi, the Hall resistivity is obtained by measuring the transverse resistivity under positive and negative fields, namely $\rho_{xy} = [\rho_{xy}(+B) - \rho_{xy}(-B)]/2$, which is used to eliminate the longitudinal resistivity contribution due to voltage probe misalignment [27]. As shown in figure 5(a), the field-dependent Hall resistivity exhibits nonlinear behavior, indicating the involvement of more than one type of charge carrier in the transport process [28, 30]. The negative/positive slopes of high-field Hall resistivity at low/high temperature suggest that the dominant carriers change from electron to hole with the increment of temperature [27, 28, 30]. Figure 5(b) plots the Hall coefficient R_H as a function of temperature at 6 T and 9 T [19], which shows a strong temperature dependence and changes its sign around 6 K. The strong nonlinear behaviors and sign changed Hall coefficient in Hall resistivity have been widely observed in several semimetals, which are interpreted as the electron–hole compensation mechanism [19, 20, 28]. Obviously, sign change of the Hall coefficient together with the quasi-quadratic magnetoresistance at low temperature illustrate that this interpretation can also be applicable to HoBi. Here, it is assumed that the carrier concentration and mobilities are insensitive to magnetic field, and the carrier concentration are well compensated. Under this assumption, the magnetoresistance, zero-field resistivity, and Hall coefficient in two-band model can be written as: $MR = [\rho(H, T) - \rho(0, T)]/\rho(0, T) = \mu_e \cdot \mu_h H^2$, $\rho(T) = 1/[n_e(\mu_e + \mu_h)]$, and $R_H = (\mu_h - \mu_e)/[n_e(\mu_e + \mu_h)]$ [19, 54]. Consequently, the obtained carrier mobilities at 2 K are $\mu_e = 1.9 \times 10^4 \text{ cm}^2 \text{ V}^{-1} \text{ s}^{-1}$ and $\mu_h = 2.6 \times 10^4 \text{ cm}^2 \text{ V}^{-1} \text{ s}^{-1}$ respectively, which are comparable to those of the Dirac semimetals HfTe_5 , TlBiSSe , and so on [55, 56]. Besides, the extracted electron and hole densities are $n_e \approx n_h = 5.3 \times 10^{21} \text{ cm}^{-3}$. Such high mobility and nearly perfect carrier compensation in HoBi could be the major cause for generation of the unprecedentedly large and quasi-quadratic magnetoresistance. Figure 5(c) shows the extracted concentrations and mobilities for both types of carriers as a function of temperature, in which both the two parameters are strongly temperature-dependent. As plotted, the mobilities of electron and hole decrease with the temperature warming up, and are comparable to each other, which suggests that the two types of carriers contribute significantly to the transport properties. This behavior is reflected in the Kohler scaling analysis as well, where magnetoresistance curves deviate from the scaling at low temperature.

3.5. Band structure calculations

As presented above, high magnetic field drives the emergence of a particular case instead of the generally plain quadratic magnetoresistance curves expected in many other semimetals, which has been scarcely reported [18, 29, 36]. Therefore, an in-depth study on electronic structure of the ferromagnetic phase of HoBi could help to understand the origin of extreme magnetoresistance in rare earth monopnictide family. The bulk band structure of ferromagnetic phase (figure 6) is calculated by the GGA method without and with SOC effect respectively. Figure 6(a) shows the partial density of states (PDOS) of the ferromagnetic state of HoBi, from which it can be observed that the f -electrons of Ho fully localize at non-occupied states near the Fermi level and the valence and conduction bands are mainly dominated by Bi- $6p$ and Ho- $5d$. Figure 6(b) illustrates the obtained energy band structure without SOC for HoBi, in which there are a few bands crossing the Fermi level and the valence and conduction bands clearly dip into each other along the high-symmetry Γ -X line, suggesting the semimetal features without band crossing points. Similar to those reported for lanthanum monopnictides, double degenerate bands with a gap of 0.19 eV develop at the X-point, which leads to the proposal of two-dimensional topologically nontrivial states [57]. It is common knowledge that in Bi-based compounds the effect

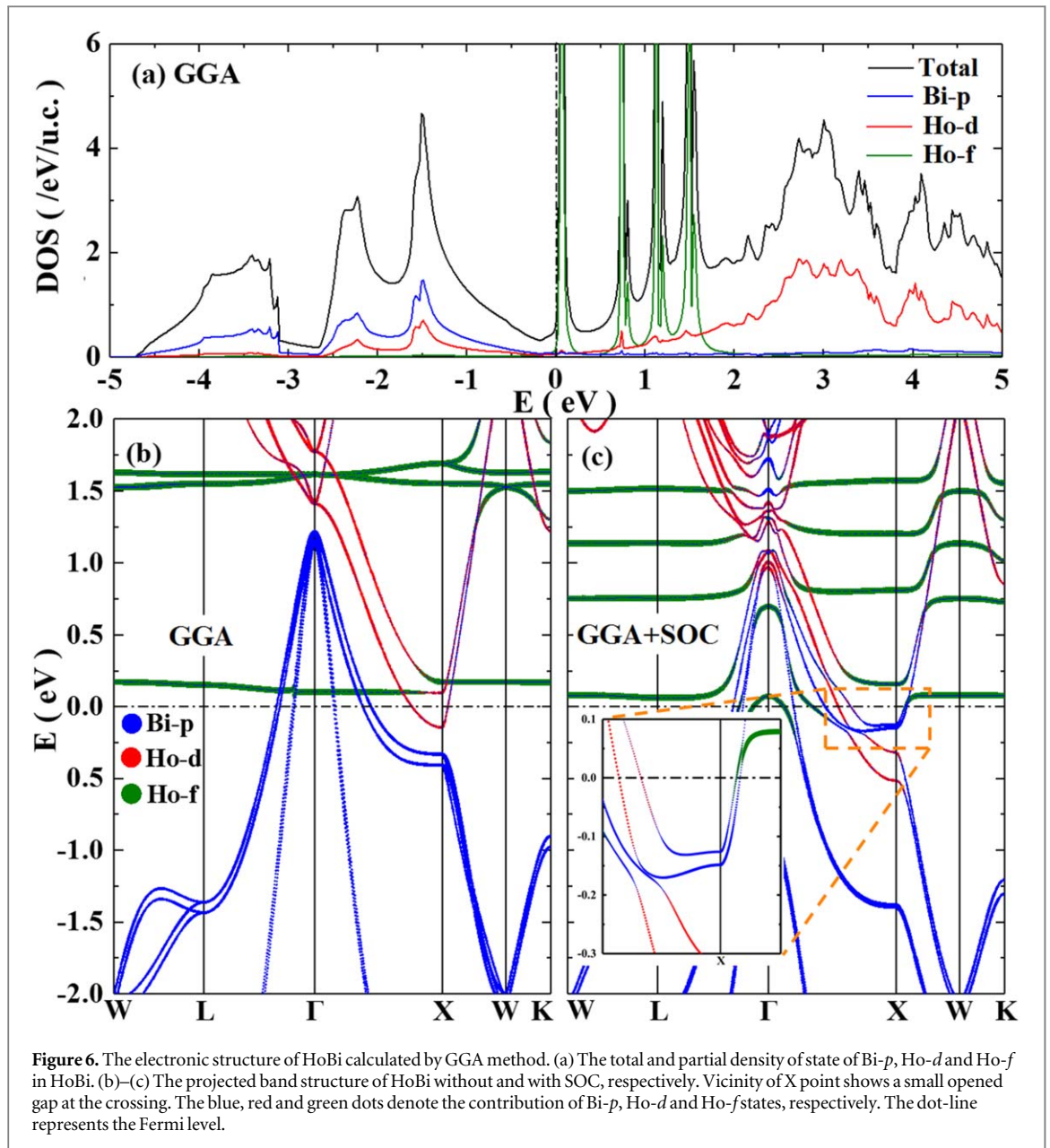
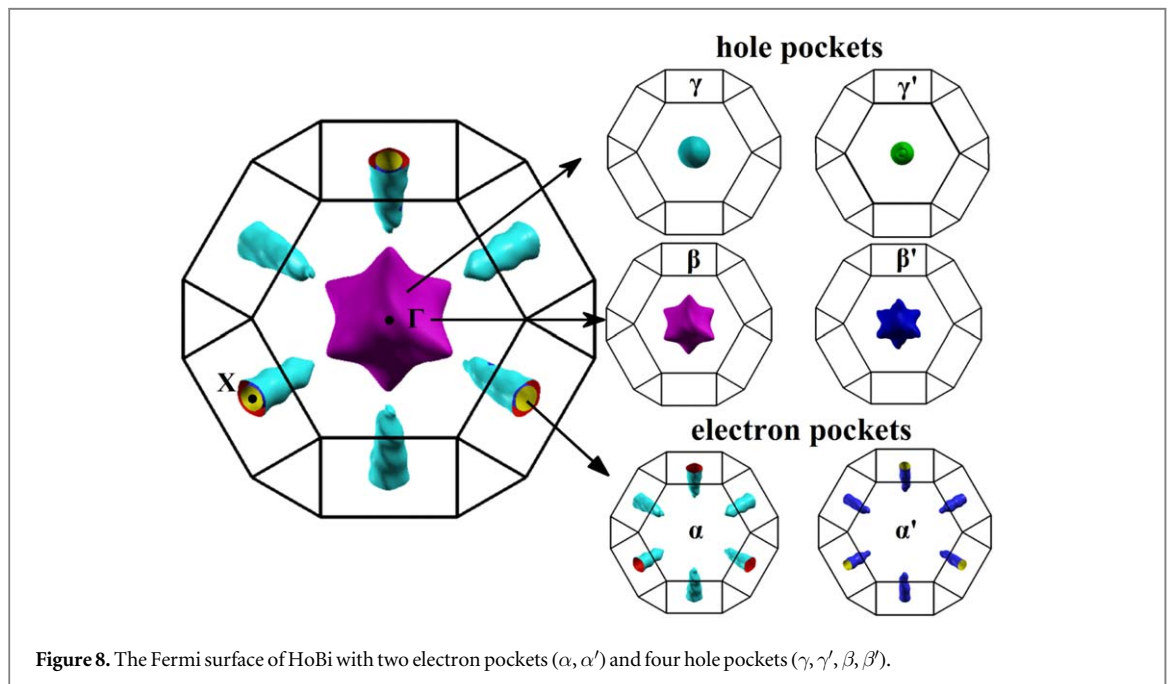
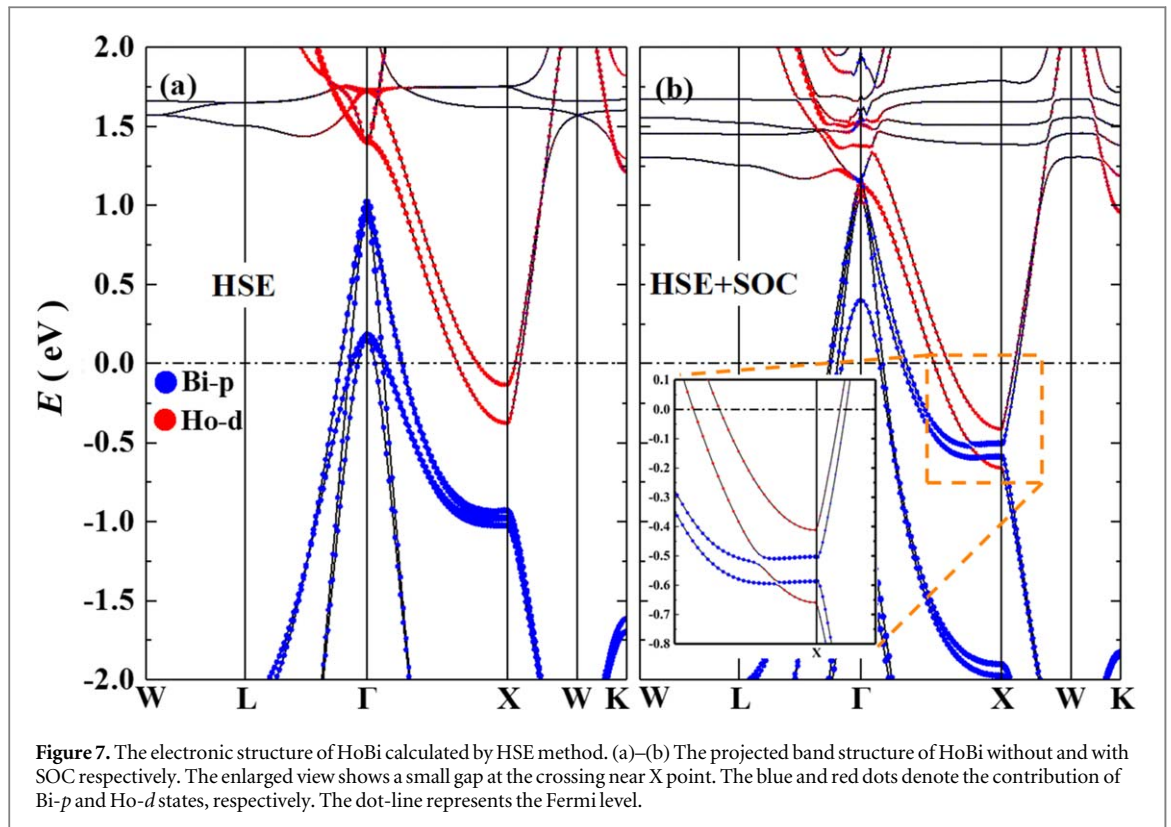


Figure 6. The electronic structure of HoBi calculated by GGA method. (a) The total and partial density of state of Bi- p , Ho- d and Ho- f in HoBi. (b)–(c) The projected band structure of HoBi without and with SOC, respectively. Vicinity of X point shows a small opened gap at the crossing. The blue, red and green dots denote the contribution of Bi- p , Ho- d and Ho- f states, respectively. The dot-line represents the Fermi level.

of SOC is very dramatic and shouldn't be ignored for band structure calculation with potential topological nature [28]. Indeed, as shown in figure 6(c), possibly due to the relativistic effect, more complicated electronic structures develop, where the sixfold degeneracy of Bi- $6p$ states is modified at Γ point, namely, four of the p bands dip deeply around the Fermi level with the other two p bands still degenerated. Furthermore, twofold degeneracy of the two bands is gradually lifted along Γ -L and Γ -X direction, and they are well separated at L- and X-points. Noticeably, the band crossing points forming by Ho- $5d$ and Bi- $6p$ states (visualized with red and blue colors in the enlarged drawing of figure 6(c)) at X-point, exhibit inverted electronic structures and a very tiny gap, where the Dirac cones may potentially generate. For HoBi, there are eight time-reversal invariant points in the body-centered-cubic Brillouin zone, including (0,0,0), (0,0,0.5), (0,0.5,0), (0,0.5,0.5), (0.5,0,0), (0.5,0,0.5), (0.5,0.5,0) and (0.5,0.5,0.5). Due to the cubic crystal symmetry, the parity criteria proposed by Fu and Kane is employed to calculate the Z_2 index for determining the topological features [58]. The topological index is rigorously evaluated from the parity of valence band wave functions at each time-reversal invariant momentum and can be identified as (1; 000), which indicates that HoBi has nontrivial electronic structures and is a topological semimetal candidate.

For better estimating the band gap as well as the band topologies of HoBi [28], the electronic structures are also checked by the HSE06 hybrid functional calculation without and with SOC interactions. Here, the discussion mainly focuses on the band structure around Fermi level. As shown in figure 7(a), the band topologies obtained through the hybrid calculation without SOC also show no band inversion along the Γ -X line, in which a larger gap (comparing to that in figure 6(b)) about 0.55 eV is observed. Agreeing with figure 6(c), the band gap



will be closed when SOC effect is included, resulting in inverted electronic structures in a deeper position with two crossing points near the X-point (figure 7(b)). Besides, smaller gaps are obtained in the magnified region of band crossing points from HSE06 method. Through further comparison of the band structures in figure 7, it can be found that hole occupy states dominate the electronic structure around the Fermi level in the case without SOC, which deviates from the experimental observation of electron–hole compensation behavior, indicating that this relativistic effect plays an important role in determining the band structure of HoBi. Sincerely, the band structures calculated by HSE06 are slightly different from those obtained from GGA method, which seems to be inevitable. While, the compensated and inverted band structures still can be obtained, as plotted in figure 7(b), confirming again that HoBi is a semimetal candidate and hosts Z_2 topological nature.

Based on the GGA and HSE06 calculations, a schematic illustration of the *fcc* Brillouin zone of HoBi can be extracted. The band calculations reveal that there are two electron pockets and four hole pockets (figure 8) in the first Brillouin zone. The electron pockets (α and α') are strongly anisotropic and locate at *X* points. While, the hole pockets (γ and γ') are identical in shape with the other two anisotropic hole pockets (β and β') being entirely wrapped at the Γ point. All pockets have only one extremal orbit supporting that the magnetic field is applied along the crystallographic axes. By rough assessment, it is found that the volumes of electron and the hole pockets are comparable, which verifies the semimetal nature of HoBi.

4. Conclusion

To summarize, we confirm that the existence of successive magnetic transitions and extreme magnetoresistance in HoBi single crystal grown by Bi flux. Two-band model analysis of magnetoresistance suggests that HoBi is a compensated semimetal, which is similar to other members of rare earth monpnictide family. Hall resistivity measurement indicates that the carrier mobility in HoBi is ultrahigh. The challenges of band structure calculations for semimetals with small Fermi surfaces are highlighted by GGA and HSE06 methods. Both the two calculations reveal that the electronic structure hosts compensated and nontrivial features in ferromagnetic state, which indicates that HoBi is a potential topological semimetal candidate. The electron–hole compensation and high mobility are suggested to be responsible for the occurrence of extremely large magnetoresistance in HoBi.

Acknowledgments

This work is supported by the National Natural Science Foundation of China (Grant No. 11604027, 11874113, 61604021 and U1832147), Natural Science Foundation of Jiangsu Province (Grants No. BK20150392), Natural Science Foundations of Fujian Province of China (Grant No. 2017J06001).

ORCID iDs

L Zhang  <https://orcid.org/0000-0003-3827-5563>

Y Fang  <https://orcid.org/0000-0002-9218-5537>

J-M Zhang  <https://orcid.org/0000-0002-0356-5387>

R J Tang  <https://orcid.org/0000-0001-6335-2095>

References

- [1] Manipatruni S, Nikonov D E and Young I A 2018 *Nat. Phys.* **14** 338
- [2] Lu C L, Gao B, Wang H W, Wang W, Yuan S L, Dong S and Liu J M 2018 *Adv. Funct. Mater.* **28** 1706589
- [3] Shkurdoda Y O, Dekhtyaruk L V, Basov A G, Chornous A M, Shabelnyk Y M, Kharchenko A P and Shabelnyk T M 2019 *J. Magn. Magn. Mater.* **477** 88
- [4] Xu X D, Mukaiyama K, Kasai S, Ohkubo T and Hono K 2018 *Acta Mater.* **161** 360
- [5] Ikhtiar S H, Xu X, Belmoubarik M, Lee H, Kasai S and Hono K 2018 *Appl. Phys. Lett.* **112** 022408
- [6] Chen F C, Lv H Y, Luo X, Lu W J, Pei Q L, Lin G T, Han Y Y, Zhu X B, Song W H and Sun Y P 2016 *Phys. Rev. B* **94** 235154
- [7] Singha R, Pariari A K, Satpati B and Mandal P 2017 *Proc. Natl Acad. Sci. USA* **114** 2468
- [8] Yang F Y, Liu K, Chien C L and Searson P C 1999 *Phys. Rev. Lett.* **82** 3328
- [9] Ali M N et al 2014 *Nature* **514** 205
- [10] Liang T, Gibson Q, Ali M N, Liu M, Cava R J and Ong N P 2015 *Nat. Mater.* **14** 280
- [11] Huang X et al 2015 *Phys. Rev. Lett.* **115** 031023
- [12] Gao W et al 2017 *Phys. Rev. Lett.* **118** 256601
- [13] Singha R, Roy S, Pariari A, Satpati B and Mandal P 2019 *Phys. Rev. B* **99** 035110
- [14] Hirschberger M, Kushwaha S, Wang Z, Gibson Q, Liang S, Belvin C A, Bernevig B A, Cava R J and Ong N P 2016 *Nat. Mater.* **15** 1161
- [15] Shekha C et al 2018 *Proc. Natl Acad. Sci. USA* **115** 9140
- [16] Tafti F F, Gibson Q D, Kushwaha S K, Haldolaarachchige N and Cava R J 2016 *Nat. Phys.* **12** 272
- [17] Wu F, Guo C Y, Smidman M, Zhang J L and Yuan H Q 2017 *Phys. Rev. B* **96** 125122
- [18] Guo C, Cao C, Smidman M, Wu F, Zhang Y, Steglich F, Zhang F C and Yuan H 2017 *NPJ Quantum Mater.* **2** 39
- [19] Song J J, Tang F, Zhou W, Fang Y, Yu H L, Han Z D, Qian B, Jiang X F, Wang D H and Du Y W 2018 *J. Mater. Chem. C* **6** 3026
- [20] Wang Y Y, Zhang H, Lu X Q, Sun L L, Xu S, Lu Z Y, Liu K, Zhou S and Xia T L 2018 *Phys. Rev. B* **97** 085137
- [21] Xu J, Ghimire N J, Jiang J S, Xiao Z L, Botana A S, Wang Y L, Hao Y, Pearson J E and Kwok W K 2017 *Phys. Rev. B* **96** 075159
- [22] Pavlosiuk O, Kleinert M, Swatek P, Kaczorowski D and Wiśniewski P 2017 *Sci. Rep.* **7** 12822
- [23] Hu Y J, Aulestia P E I, Tse K F, Kuo C N, Zhu J Y, Lue C S, Lai K T and Goh Swee K 2018 *Phys. Rev. B* **98** 035133
- [24] Liang D D, Wang Y J, Xi C Y, Zhen W L, Yang J, Pi L, Zhu W K and Zhang C J 2018 *APL Mater.* **6** 086105
- [25] Zhou Y et al 2017 *Phys. Rev. B* **96** 205122
- [26] Wang Y et al 2018 *Phys. Rev. B* **97** 115133
- [27] Sun S, Wang Q, Guo P J, Liu K and Lei H 2016 *New J. Phys.* **18** 082002

- [28] Qian B, Tang F, Ruan Y R, Fang Y, Han Z D, Jiang X F, Zhang J M, Chen S Y and Wang D H J *Mater. Chem. C* **6** 10020
- [29] Yang H Y, Gaudet J, Aczel A A, Graf D E, Blaha P, Gaulin B D and Tafti F 2018 *Phys. Rev. B* **98** 045136
- [30] Pavlosiuk O, Swatek P, Kaczorowski D and Wiśniewski P 2018 *Phys. Rev. B* **97** 235132
- [31] Petit L, Szotek Z, Lüders M and Svane A 2016 *J. Phys. Condens. Matter* **28** 223001
- [32] Zeng M G, Fang C, Chang G Q, Chen Y A, Hsieh T, Bansil A, Lin H and Fu L 2015 arXiv:1504.03492
- [33] Nayak J et al 2017 *Nat. Commun.* **8** 13942
- [34] Wan X, Turner Ari M, Vishwanath A and Savrasov Sergey Y 2011 *Phys. Rev. B* **83** 205101
- [35] Xu G, Weng H, Wang Z, Dai X and Fang Z 2011 *Phys. Rev. Lett.* **107** 186806
- [36] Wang Y Y, Sun L L, Xu S, Su Y and Xia T L 2018 *Phys. Rev. B* **98** 045137
- [37] Kuroda K et al 2018 *Phys. Rev. Lett.* **120** 086402
- [38] Li Z, Xu D D, Ning S Y, Su H, Iitaka T, Tohyama T and Zhang J X 2017 *Int. J. Mod. Phys. B* **31** 1750217
- [39] Hulliger F, Ott H R and Siegrist T 1984 *J. Less-Common Met.* **96** 263
- [40] Fente A, Suderow H, Vieira S, Nemes N M, García-Hernández M, Bud'ko S L and Canfield P C 2013 *Solid State Commun.* **171** 59
- [41] Kresse G and Hafner J 1993 *Phys. Rev. B* **48** 13115
- [42] Perdew J P, Burke K and Ernzerhof M 1996 *Phys. Rev. Lett.* **77** 3865
- [43] Heyd J, Scuseria G E and Ernzerhof M 2003 *J. Chem. Phys.* **118** 8207
- [44] Yue X Y, Ouyang Z W, Wang J F, Wang Z X, Xia Z C and He Z Z 2018 *Phys. Rev. B* **97** 054417
- [45] Busch G and Vogt O 1967 *Phys. Lett. A* **25** 449
- [46] Luo X et al 2018 *Phys. Rev. B* **97** 205132
- [47] Sankar R, Peramaiyan G, Muthuselvam I P, Xu S, Hasan M Z and Chou F C 2017 *J. Phys. Condens. Matter* **30** 015803
- [48] Pariari A, Singha R, Roy S, Satpati B and Mandal P 2018 *Sci. Rep.* **8** 10527
- [49] Wang Y L et al 2015 *Phys. Rev. B* **92** 180402
- [50] Zeng L K et al 2016 *Phys. Rev. Lett.* **117** 127204
- [51] Fu D, Pan X, Bai Z, Fei F, Umana-Membreno G A, Song H, Wang X, Wang B and Song F 2018 *Nanotechnology* **29** 135705
- [52] Melnikov M Y, Shashkin A A, Dolgoplov V T, Huang S H, Liu C W and Kravchenko S V 2015 *Appl. Phys. Lett.* **106** 092102
- [53] Ali M N, Schoop L, Xiong J, Flynn S, Gibson Q, Hirschberger M, Ong N P and Cava R J 2015 *Europhys. Lett.* **110** 67002
- [54] Li D X, Haga Y, Shida H and Suzuki T 1996 *Phys. Rev. B* **54** 10483
- [55] Wang H et al 2016 *Phys. Rev. B* **93** 165127
- [56] Novak M, Sasaki S, Segawa K and Ando Y 2015 *Phys. Rev. B* **91** 041203
- [57] Pavlosiuk O, Swatek P and Wiśniewski P 2016 *Sci. Rep.* **6** 38691
- [58] Fu L and Kane C L 2007 *Phys. Rev. B* **76** 045302